J. Indian Inst. Sci., Nov.–Dec. 2005, **85**, 353–365

Pulsed nozzle Fourier transform microwave spectroscopic and *ab initio* investigations on the weakly bound Ar-$(H_2S)_2$ trimer

PANKAJ K. MANDAL, MAUSUMI GOSWAMI AND E. ARUNAN*
Department of Inorganic and Physical Chemistry, Indian Institute of Science, Bangalore 560 012, India.
email: arunan@ipc.iisc.ernet.in

Received on May 9, 2005; Revised on August 2, 2005.

Abstract

A pulsed nozzle Fourier transform microwave spectrometer has been used to obtain the rotational spectra of Ar-$(H_2S)_2$ and Ar-$(D_2S)_2$ trimers. Two states have been observed for each trimer and these are likely to arise due to tunneling/internal rotation of the two H_2S monomers within the trimer. The rotational constants for the lower state of Ar-$(H_2S)_2$ are: A = 1810.410(6) MHz; B = 1596.199(9) MHz and C = 848.814(2) MHz; and those for Ar-$(D_2S)_2$ are A = 1725.49(1) MHz; B = 1566.26(2) MHz; and C = 826.818(3) MHz. From these rotational constants, the Ar-H_2S and H_2S-H_2S distances have been estimated to be 4.04 and 4.08 Å, respectively. The splitting observed between the two states is of the order of a few MHz for Ar-$(H_2S)_2$ and a few kHz for Ar-$(D_2S)_2$. *Ab initio* calculations at MP2 level with large basis sets up to aug-cc-PVQZ level lead to three different minima, including a pseudo-linear one. Experimental rotational constants are consistent with the other two T-shaped structures in which Ar approaches the $(H_2S)_2$ along either its B or C axis. Single-point calculations at CCSD(T)/aug-cc-pVTZ level identifies the global minimum as having Ar along the B/C axis of $(H_2S)_2$ and it has a stabilization energy of 1.0 kcal mol^{-1}, after zero-point and counter-poise corrections.

Keywords: Weakly bound complexes, intermolecular interactions, spectroscopic methods.

1. Introduction

Weakly bound complexes formed in a supersonic expansion have attracted significant attention in the past few decades. The main goal of these studies is improving our understanding of intermolecular interactions that control the behaviour in bulk. Coupling of supersonic expansion with various spectroscopic methods has vastly helped in obtaining accurate experimental data on these complexes [1, 2]. Rotational spectroscopy [3, 4] is useful in giving accurate equilibrium structure of the complexes, which is the first step towards the complete determination of intermolecular potentials. Towards this objective, the pulsed nozzle Fourier transform microwave (PNFTMW) spectrometer has played a dominant role [5, 6].

Complexes containing rare gases have found a prominent place as models for inductive and dispersive forces in intermolecular interactions. It is important to look beyond dimeric complexes such as A_2 or AB and get experimental data on A_mB_n complexes, for a thorough understanding of the interactions in bulk. With this goal in mind, rotational spectra of a series of Rg_m-HX (Rg = rare gas; m = 1–3 and X = halogen) complexes have been reported [7], starting with the first report on Ar-HCl[8] dimer in 1973. In comparison, studies on Rg_m-

*Author for correspondence.

H_2Y (Y = O/S) [9–11] complexes started more than a decade later. However, somewhat intriguingly, there has not been any report on the rotational spectra of Rg-$(HX)_n$ complexes yet. On the other hand, rotational spectra of Ar-$(H_2O)_n$ (n = 2–3) complexes have already been reported [12, 13]. In this manuscript, rotational spectrum of the weakly bound Ar-$(H_2S)_2$ complex, obtained using a PNFTMW spectrometer, is reported.

The Ar-$(H_2S)_2$ complex is interesting for several reasons. Often H_2O and H_2S are compared to highlight the importance of hydrogen bonding [14]. The boiling points and melting points for the two molecules differ significantly. Hence, historically it was believed that H_2O forms hydrogen bonds and H_2S does not. However, now it is well established that C–H and S–H groups can also form hydrogen bonds, though they are not as strong as the hydrogen bonds formed by the traditional hydrogen bond donors such as N–H, O–H and F–H [15]. Recently, we reported the rotational spectrum and structure of the C_2H_4–H_2S complex [16], which has an equilibrium geometry that is very similar to that of C_2H_4–H_2O. Our laboratory is presently investigating a series of H_2S complexes for comparison with analogous H_2O complexes and Ar-$(H_2S)_2$ results are presented here. Such comparisons will be important in understanding the differences observed in bulk. *Ab initio* calculations have been carried out at MP2 and CCSD levels with large basis sets (up to aug-cc-pVTZ) on Ar-$(H_2S)_2$ and $(H_2S)_2$ and the results are reported here.

2. Experimental details

The pulsed nozzle Fourier transform microwave spectrometer used in this study has been described in detail elsewhere [17]. Briefly, the reagent gases diluted with a rare gas (Ar or He) are supersonically expanded into a Fabry–Perot cavity, made of aluminium mirrors. The Fabry–Perot cavity is housed inside a vacuum chamber which is evacuated to 10^{-6} mbar by a roots blower/diffusion pump combination. A microwave pulse is coupled to the cavity through an antenna and it produces a standing wave within the cavity if the distance between the mirrors meets the boundary conditions for the standing wave. As the source is pulsed, the standing wave has a bandwidth of about 1 MHz. The sample will be polarized if there is a rotational transition within this bandwidth. Polarized sample emits a free induction decay which is transmitted by the same antenna to a double super-heterodyne detection system. This time-domain signal is digitized and Fourier transformed to get the spectrum. The signal-to-noise ratio is improved by averaging over many cycles. One modification that has been done recently is that multiple FIDs can be collected per single gas pulse, significantly reducing the time required for averaging. This is possible as the residence time of the gas sample inside the cavity is about 2 ms but the FIDs typically last for a few hundred *m*s only. Figure 1 shows several FIDs that have been digitized during one gas pulse, for example.

The Ar-$(H_2S)_2$ was formed by co-expanding 1.0–2.0% H_2S in Ar. The identity of the complex was established by stopping the H_2S flow and by changing the carrier gas to He, both of which resulted in the loss of signal. In addition, the rotational constants determined from the fit (next section) are closer to the prediction for Ar-$(H_2S)_2$. Moreover, from the experimental rotational constants for Ar-$(H_2S)_2$, the Ar-$(D_2S)_2$ rotational constants could be predicted and observed. The D_2S was produced by bubbling H_2S through D_2O. The optimum microwave pulse was of 0.5 μs duration.

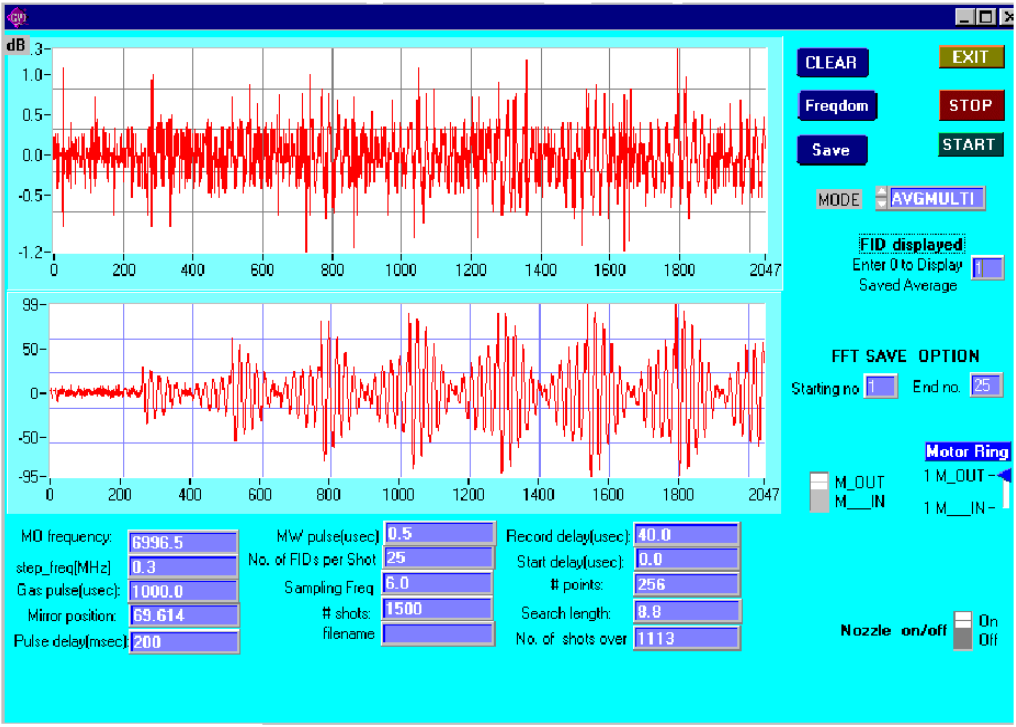

FIG. 1. Graphical user interface for the pulsed nozzle Fourier transform microwave spectrometer showing a typical time-domain signal observed with multiple FIDs per gas pulse. The upper panel shows FIDs for a particular gas pulse and the lower panel the averaged signal for several such gas pulses. A total of 8 FIDs, each having 256 points, is displayed here. The time interval between two points is ~ 166.6 ns. The signal is from $(H_2S)_2$.

3. Results and discussion

3.1. *Search and assignment*

A symmetric T-shaped heavy atom geometry has been assumed for Ar-$(H_2S)_2$ complex as a similar structure has been determined for Ar-$(H_2O)_2$ complex [13]. In the assumed geometry, which is an asymmetric top, the distance between the two H_2S units was taken to be the same as that in $(H_2S)_2$ [18]. The Ar atom was placed equidistant from both the H_2S units such that the Ar-c.m.(H_2S) distance is similar to that in Ar-H_2S complex [11, 19]. The rotational transitions, both *a* and *b* dipoles, were predicted for this assumed geometry. As the principal inertial axis parallel to the S–S bond is *b*-axis for this geometry, the *b*-dipole transitions were expected to be stronger. Hence, scanning was started for the *b*-dipole transition $2_{02} \rightarrow 3_{13}$ predicted at ~ 6025 MHz. Two strong lines were readily found at 5964.1340 and 5971.5046 MHz along with two other weaker lines at 5959.3882 and 5966.6796 MHz. The line at 5964.1340 MHz was assigned as $2_{02} \rightarrow 3_{13}$ transition and the weaker line at 5959.3882 MHz was assigned as *a*-dipole $2_{02} \rightarrow 3_{03}$ transition for Ar-$(H_2S)_2$. On the basis of these assignments, the other *a*- and *b*-dipole transitions were predicted and found readily. A total of 40 *a*- and *b*-dipole transitions have been observed for Ar-$(H_2S)_2$.

Table I
Observed transitions for both lower and upper states for Ar-$(H_2S)_2$

Transitions	Lower		Upper	
	Obs. Freq (MHz)	Res. (kHz)	Obs. Freq. (MHz)	Res. (kHz)
$2_{12} \rightarrow 3_{03}$	5919.5143	10.4	–	–
$2_{12} \rightarrow 3_{13}$	5924.2629	10.5	–	–
$2_{02} \rightarrow 3_{03}$	5959.3882	–5.1	5966.6796	–9.9
$2_{02} \rightarrow 3_{13}$	5964.1340	–7.8	5971.5046	11.1
$2_{21} \rightarrow 3_{12}$	7142.7020	–3.0	7136.2504	0.8
$3_{13} \rightarrow 4_{04}$	7635.8962	11.7	7642.0509	–19.6
$3_{13} \rightarrow 4_{14}$	7636.3661	12.9	7642.5010	2.9
$3_{03} \rightarrow 4_{04}$	7640.6394	6.4	7646.8630	–11.5
3_{03} 4 $_{14}$	7641.1092	7.5	7647.3053	3.2
$2_{11} \rightarrow 3_{22}$	7976.1100	–7.4	7996.1130	3.0
$3_{22} \rightarrow 4_{13}$	9229.0356	–1.5	–	–
$3_{22} \rightarrow 4_{23}$	9261.5525	–0.2	–	–
$4_{14} \rightarrow 5_{05}$	9335.2010	–3.2	9341.8420	–12.2
$4_{14} \rightarrow 5_{15}$	9335.2426	–3.6	9341.8820	–1.6
$4_{04} \rightarrow 5_{05}$	9335.6683	–4.7	9342.2920	10.3
$4_{04} \rightarrow 5_{15}$	9335.7076	–7.4	9342.3290	17.9
$3_{12} \rightarrow 4_{13}$	9419.9420	–0.8	9429.0690	–1.6
$3_{12} \rightarrow 4_{23}$	9452.4774	18.9	9461.9275	–4.3
$2_{20} \rightarrow 3_{31}$	9986.1125	–2.1	9998.9205	0.6
$4_{23} \rightarrow 5_{14}$	11015.9524	2.6	–	–
$4_{23} \rightarrow 5_{24}$	11020.1115	7.9	11024.9062	1.6
$5_{15} \rightarrow 6_{06}$	11032.3329	–10.1	11039.8235	–0.2
$5_{15} \rightarrow 6_{16}$	11032.3329	–13.6	11039.8235	–1.4
$5_{05} \rightarrow 6_{06}$	11032.3745	–10.5	11039.8664	13.3
$5_{05} \rightarrow 6_{16}$	11032.3745	–14.0	11039.8664	12.1
$4_{13} \rightarrow 5_{14}$	11048.4680	2.5	–	–
$4_{13} \rightarrow 5_{24}$	11052.6015	–17.7	–	–
$3_{21} \rightarrow 4_{32}$	11702.6670	0.3	–	–
$6_{16} \rightarrow 7_{07}$	12729.0515	1.0	12737.5490	–2.1
$6_{16} \rightarrow 7_{17}$	12729.0515	0.8	12737.5490	–2.0
$6_{06} \rightarrow 7_{07}$	12729.0515	–2.4	12737.5490	–3.3
$6_{06} \rightarrow 7_{17}$	12729.0515	–2.8	12737.5490	–3.2
$7_{17} \rightarrow 8_{08}$	14425.4752	13.1	14435.0073	–3.2
$7_{17} \rightarrow 8_{18}$	14425.4752	13.0	14435.0073	–3.2
$7_{07} \rightarrow 8_{08}$	14425.4752	12.8	14435.0073	–3.1
$7_{07} \rightarrow 8_{18}$	14425.4752	12.8	14435.0073	–3.1
$8_{18} \rightarrow 9_{09}$	16121.5749	–5.3	16132.1660	1.6
$8_{18} \rightarrow 9_{19}$	16121.5749	–5.3	16132.1660	1.6
$8_{08} \rightarrow 9_{09}$	16121.5749	–5.3	16132.1660	1.6
$8_{08} \rightarrow 9_{19}$	16121.5749	–5.3	16132.1660	1.6

The residues of the fits are also included. (Residue = Observed – Calculated).

Table II
Observed transitions for both Lower and Upper states for Ar-$(D_2S)_2$

Transitions	Lower		Upper	
	Obs. Freq. (MHz)	Res. (kHz)	Obs. Freq. (MHz)	Res. (kHz)
$2_{12} \rightarrow 3_{03}$	5764.0315	–2.4	5764.0640	–4.3
$2_{12} \rightarrow 3_{13}$	5766.1600	–5.2	5766.1930	–5.2
$2_{02} \rightarrow 3_{13}$	5789.2690	–6.3	5789.2990	–1.1
$3_{13} \rightarrow 4_{04}$	7428.3615	18.8	7428.3886	14.7
$3_{13} \rightarrow 4_{14}$	7428.5175	11.2	7428.5461	8.8
$3_{03} \rightarrow 4_{04}$	7430.4981	24.2	7430.5244	20.7
$3_{03} \rightarrow 4_{14}$	7430.6523	14.7	7430.6799	12.7
$2_{11} \rightarrow 3_{22}$	7656.1790	–1.8	7656.2180	0.4
$3_{22} \rightarrow 4_{13}$	9001.5100	3.4	9001.5550	0.2
$3_{22} \rightarrow 4_{23}$	9016.2330	–9.4	9016.284	–3.1
$4_{14} \rightarrow 5_{05}$	9082.4446	–3.6	9082.4785	–3.5
$4_{14} \rightarrow 5_{15}$	9082.4446	–15.1	9082.4785	–14.9
$4_{04} \rightarrow 5_{05}$	9082.6086	–3.3	9082.6429	–2.6
$4_{04} \rightarrow 5_{15}$	9082.6086	–14.8	9082.6429	–14.0
$3_{12} \rightarrow 4_{13}$	9113.9930	0.9	9114.0160	–9.6
$3_{12} \rightarrow 4_{23}$	9128.7280	0.0	9128.7600	2.1
$2_{20} \rightarrow 3_{31}$	9522.5860	–0.2	9522.6550	0.3
$4_{23} \rightarrow 5_{14}$	10706.4090	0.0	10706.4500	2.3
$4_{23} \rightarrow 5_{24}$	10707.8705	0.5	10707.9135	5.4
$4_{13} \rightarrow 5_{14}$	10721.1480	3.3	10721.182	2.0
$4_{13} \rightarrow 5_{24}$	10722.6070	1.2	10722.6410	5.5
$5_{15} \rightarrow 6_{06}$	10735.4942	–1.8	10735.5324	–2.4
$5_{15} \rightarrow 6_{16}$	10735.4942	–2.5	10735.5324	–3.2
$5_{05} \rightarrow 6_{06}$	10735.4942	–13.3	10735.5324	–13.9
$5_{05} \rightarrow 6_{16}$	10735.4942	–14.0	10735.5324	–14.7
$5_{24} \rightarrow 6_{15}$	12364.8730	3.5	12364.9170	1.3
$5_{24} \rightarrow 6_{25}$	12364.9910	–3.6	12365.0390	–1.8
$5_{14} \rightarrow 6_{15}$	12366.3325	1.9	12366.3775	1.3
$5_{14} \rightarrow 6_{25}$	12366.4540	–1.7	12366.4980	–3.2
$6_{16} \rightarrow 7_{07}$	12388.2940	6.3	12388.3420	9.0
$6_{16} \rightarrow 7_{17}$	12388.2940	6.3	12388.3420	8.9
$6_{06} \rightarrow 7_{07}$	12388.2940	5.6	12388.3420	8.2
$6_{06} \rightarrow 7_{17}$	12388.2940	5.5	12388.3420	8.2
$7_{17} \rightarrow 8_{08}$	14040.8390	–1.8	14040.8920	–1.4
$7_{17} \rightarrow 8_{18}$	14040.8390	–1.8	14040.8920	–1.4
$7_{07} \rightarrow 8_{08}$	14040.8390	–1.9	14040.8920	–1.4
$7_{07} \rightarrow 8_{18}$	14040.8390	–1.9	14040.8920	–1.4
$8_{18} \rightarrow 9_{09}$	15693.1205	1.0	15693.1790	–0.2
$8_{18} \rightarrow 9_{19}$	15693.1205	1.0	15693.1790	–0.2
$8_{08} \rightarrow 9_{09}$	15693.1205	1.0	15693.1790	–0.2
$8_{08} \rightarrow 9_{19}$	15693.1205	1.0	15693.1790	–0.2

The residues of the fits are also included. (Residue = Observed – Calculated).

Even after the complete assignment of these transitions, many lines were left unassigned (e.g. 5971.5046 and 5966.6796 MHz). Most of them are very close to the assigned transi-

tions for Ar-$(H_2S)_2$ and need similar optimum conditions to be observed. These lines could be fitted as another set of transitions where the lines at 5971.5046 and 5966.6796 MHz are assigned as $2_{02} \rightarrow 3_{13}$ and $2_{02} \rightarrow 3_{03}$ transitions, respectively. A total of 32 *a*- and *b*-dipole transitions have been observed and assigned for this series of transitions. Both sets of transitions are listed in Table I along with the residues from the fit. These two sets of transitions correspond to two different tunneling/internal rotor states of Ar-$(H_2S)_2$ and are designated as the lower and upper states. The upper state transition frequencies are higher than those corresponding to lower state transitions. A similar two-state pattern in rotational spectra has been observed for $(H_2S)_2$ dimer also [18]. No other set of transitions could be assigned yet.

The search for the Ar-$(D_2S)_2$ spectra was quiet straightforward as the rigid rotor prediction from the Ar-$(H_2S)_2$ rotational constants gave rotational constants very close to the experimental values. A total of 41 transitions, *a*- and *b*-dipole, have been observed for each tunneling/internal rotor state of Ar-$(D_2S)_2$. For this isotopomer both the states are very close to each other and could be seen in a single window. The observed transitions and their residues are listed in Table II. The quadrupole hyperfine splitting due to the four D nuclei could not be resolved.

For both the isotopomers, the *b*-dipole transitions are stronger than the *a*-dipole ones. This indicates that the dipole moment component along the *b* inertial axis of the complex is higher than that on the *a*-axis. Both sets of transitions for Ar-$(H_2S)_2$ and Ar-$(D_2S)_2$ have been fitted independently to the Watson Hamiltonian [20] for distorted asymmetric rotor with A reduction. The fitted rotational and centrifugal distortion constants are shown in Table III along with standard deviations of the fits. For all the four series of transitions, the standard deviations are within 7–9 kHz. However, for Ar-$(H_2S)_2$, six distortion terms are needed in the fit, H_J being the only sextet term, whereas using only five quartic distortion

Table III
Fitted rotational and centrifugal distortion constants and inertial defect for Ar-$(H_2S)_2$ and Ar-$(D_2S)_2$. Standard deviation (SD) and the number of transitions (#) fitted are included too

Parameters	Ar-$(H_2S)_2$		Ar-$(D_2S)_2$	
	Lower	Upper	Lower	Upper
A (MHz)	1810.410 (6)	1826.18 (2)	1725.49 (1)	1725.52 (1)
B	1596.199 (9)	1605.94 (6)	1566.26 (2)	1566.32 (2)
C	848.814 (2)	847.11 (1)	826.818 (3)	826.814 (3)
$Ä_J$ (kHz)	20.4 (4)	323 (2)	9.5 (7)	11.1 (7)
$Ä_{JK}$	–32 (1)	–399 (6)	–12 (2)	–15 (2)
$Ä_K$	82.4 (7)	1045 (4)	26 (1)	28 (1)
d_J	8.4 (2)	153 (1)	4.1 (4)	4.8 (4)
d_K	38.9 (4)	746 (4)	6.3 (9)	8.3 (8)
$\Delta (= I_c - I_a - I_b)^a$	–0.37	5.16	–4.32	–4.30
SD (kHz)	8.7	7.4	7.8	7.4
#	40	32	41	41

[a]Inertial defect (in amu. Å^2) will be zero for a rigid-planar molecule; will be negative if the molecule/complex is nonplanar.

terms gives a reasonably good fit for Ar-$(D_2S)_2$. The uncertainties associated with the fitted parameters are quite reasonable. The distortion constants for lower and upper states of Ar-$(H_2S)_2$ have the same sign. However, the values for the upper state are about an order of magnitude higher than the corresponding lower state distortion constants. For Ar-$(D_2S)_2$ both the states have very similar distortion constants.

3.2. *Structure from experimental rotational constants*

The rotational spectra observed and the fitted rotational constants of Ar-$(H_2S)_2$ match very well with the assumed asymmetric top geometry, a T-shaped heavy atom geometry. The vibrationally averaged structure, along with its principal inertial axis system, is shown in Fig. 2. The three rotational constants obtained from the experimental spectrum are used here to estimate the Ar-H_2S and H_2S–H_2S distances, treating H_2S as a unit mass. The inertial defect for the ground state of Ar-$(H_2S)_2$ is small, justifying such a treatment (see Table III). Besides, accurate determination of the orientation of the two H_2S monomers is not possible with this data. The intermolecular separations can be determined using the following inertial equations:

$$I_a = m_{H_2S} r^2/2; \tag{1}$$

$$I_b = m_c R^2. \tag{2}$$

Here, m_{H_2S} is the mass of H_2S unit, r, the c.m. distance between the two H_2S units, m_c, the reduced mass $[2m_{H_2S} * m_{Ar}/(2m_{H_2S} + m_{Ar})]$ of the complex and R, the distance between Ar and c.m. of $(H_2S)_2$ moiety (if the inertial defect indeed is zero, $I_a + I_b = I_c$) From eqn (1), using the lower state rotational constants of Ar-$(H_2S)_2$, the r value is determined to be 4.053 Å. The upper state constants give rise to a value of 4.035 Å, whereas the Ar-$(D_2S)_2$ constants

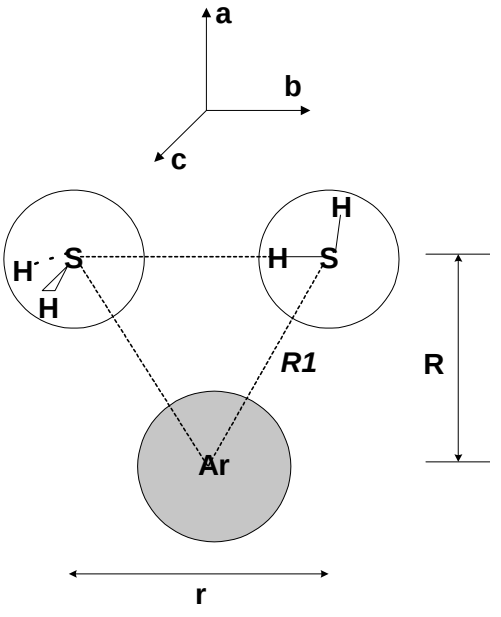

FIG. 2. Vibrationally averaged geometry of Ar-$(H_2S)_2$ obtained from spectroscopic constants. r is the c.m. distance between two H_2S units and R, the distance between Ar and c.m. of $(H_2S)_2$ moiety. R1 is the distance between Ar and c.m. of (H_2S).

Table IV
The structural parameters determined from the experimental rotational constants for lower and upper states of Ar-$(H_2S)_2$ and Ar-$(D_2S)_2$. The parameters are defined in Fig. 2. The distances are given in Å

Parameters	Ar-$(H_2S)_2$		Ar-$(D_2S)_2$		Ar-H_2S	$(H_2S)_2$
	Lower	Upper	Lower	Upper		
r	4.053	4.035	4.034	4.034	–	4.12
R	3.547	3.536	3.543	3.543	–	–
*R*1	4.085	4.071	4.077	4.077	4.01	–

(both lower and upper states) give a value of 4.034 Å. This may be compared to the intermolecular separation of 4.12 Å in $(H_2S)_2$ [18]. A similar reduction in intermolecular separation was found between $(H_2O)_2$ and Ar-$(H_2O)_2$ [13]. Equation (2) leads to *R* values of 3.547 Å and 3.536 Å, respectively for the lower and upper states of Ar-$(H_2S)_2$. The rotational constants for the deuteriated isotopomer give an *R* value of 3.543 Å. These values correspond to Ar-c.m(H_2S) (R1) distances of 4.085, 4.071 and 4.077 Å, respectively, and are marginally larger than the Ar-H_2S distance determined for the Ar-H_2S dimer, 4.01 Å. All the structural parameters obtained for both states of Ar-$(H_2S)_2$ and Ar-$(D_2S)_2$ are given in Table IV. The inertial defects for the lower and upper states of both the isotopomers give an important insight into the structure of the complex in its different tunneling/internal rotor states. For Ar-$(H_2S)_2$ the lower state has a very small negative inertial defect, whereas the upper state has a large positive value. The positive inertial defect indicates that contribution from in-plane vibrations dominate the inertial defect [4]. Both states of the per-deutoriated species have a large negative Δ (-4.3 Å^2). It is likely that the contribution from the increased mass of the out-of-plane nuclei dominates in this case.

3.3. *Ab initio calculations*

Ab initio calculations were performed at different levels of theory to optimize the Ar-$(H_2S)_2$ geometry and to determine the interaction energy. The computation was started with the $(H_2S)_2$, the precursor of Ar-$(H_2S)_2$. The global minimum of $(H_2S)_2$ has been optimized at MP2 level using different basis sets. An Ar atom can approach $(H_2S)_2$ from several orientations to form the trimer, Ar-$(H_2S)_2$. Here, we consider Ar approaching the $(H_2S)_2$ along its three principal axes to find the global minimum and any other local minima at MP2 level using different basis sets. Frequency calculations were performed to confirm the nature of the stationary points found. CCSD(T) single-point energies were calculated for all the MP2 optimized geometries using the same basis set. All the calculations were performed using Gaussian 98 software package [21].

3.3.1. *Geometry optimization*

Hydrogen sulphide dimer was optimized first at MP2 level using 6-311++G**, 6-311++G(3df,2p), aug-cc-pVTZ and aug-cc-pVQZ basis sets. The global minimum has a linear hydrogen bonded structure as shown in Fig. 3. The Ar atom can approach $(H_2S)_2$

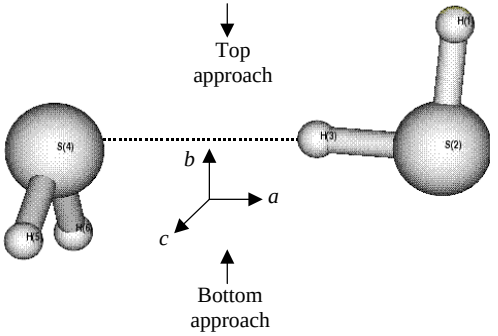

FIG. 3. Optimized geometry of $(H_2S)_2$ at MP2/aug-cc-pVTZ level of theory.

along its *a*, *b* or *c*-axis to form Ar-$(H_2S)_2$. There are two ways for Ar atom to approach $(H_2S)_2$ along its B inertial axis, from the top or bottom (see Fig. 3). Approach from the top produced a saddle point with one imaginary frequency; however, approach from the bottom resulted in a minimum (Structure A) at MP2/6-311++G(3df,2p) and MP2/aug-cc-pVTZ levels of theory. At MP2/6-311++G** level, however, this geometry could not be optimized even after 100 steps starting from the initial geometry. Another geometry (Structure B) could be optimized in

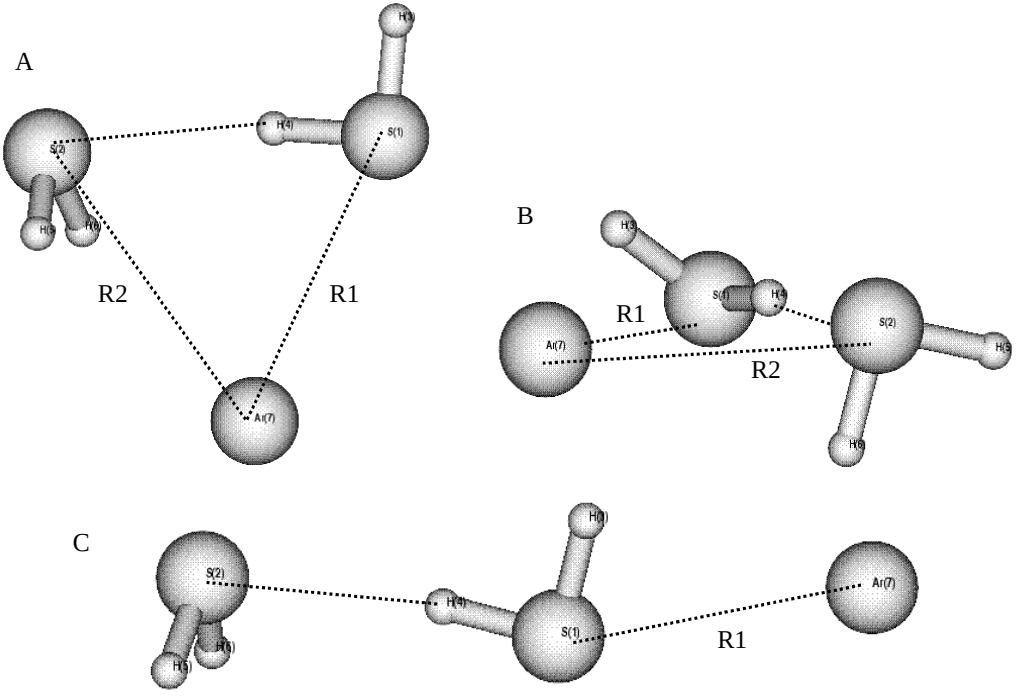

FIG. 4. Geometries of the three minima optimized at MP2/aug-cc-pVTZ level of theory. Structure A has the highest stabilization energy after BSSE correction. However, on zero point energy correction over the CP corrected interaction energy (ΔE^{ZPE}), structure B becomes the most stable. At CCSD(T)/aug-cc-pVTZ level of calculations, the ΔE^{ZPE} for the structures A, B and C is – 0.98, – 1.0 and – 0.79 kcal/mol, respectively.

Table V
The structural parameters (intermolecular distances) and the inertial defects for three minima optimized at different levels of theory. The structural parameters are defined in Fig. 2. The distances are in Å and inertial defects are in amu.Å^2

Structure		6–311++G**	6–311++G(3df,2p)	aug–cc–pVTZ	aug–cc–pVQZ
A	*r*	–	4.1164	4.0686	4.0664
	*R*1	–	3.6946	3.6581	3.6565
	*R*2	–	4.0651	3.9727	3.9709
	Δ	–	–3.73	–3.74	–3.68
B	*r*	4.1668	4.1159	4.0683	—
	*R*1	4.1848	4.1344	4.05435	—
	*R*2	3.8208	3.6883	3.6340	—
	Δ	–4.71	–4.71	–4.04	—
C	*r*	4.1745	4.1256	4.0775	4.0840
	*R*1	3.8470	3.6941	3.6643	3.6456
	Δ	–4.57	–4.31	–3.75	–3.77
r in $(H_2S)_2$		4.1725	4.1272	4.0765	4.0751

which Ar lies along the *c* inertial axis of $(H_2S)_2$. Argon approaching along *a*-axis of $(H_2S)_2$ has again two possibilities. No minimum was found in which Ar interacts with the H-bond acceptor H_2S. However, a pseudo-linear local minimum (Structure C) has been found in which the Ar interacts with the H-bond donor H_2S. In all these cases, a full geometry optimization was carried out. All the parameters were allowed to be optimized.

All three minima optimized at MP2/aug-cc-pVTZ level of theory are shown in Fig. 4. The structural parameters calculated at different levels for all three minima are given in Table V. In structure A, two hydrogens of the acceptor H_2S subunit are directed towards the Ar. Ar is closer to the donor H_2S compared to the acceptor H_2S, the Ar-S distances being 3.6581 (R1) and 3.9727 Å (R2), respectively, at MP2/aug-cc-pVTZ level of theory. In contrast to structure A, Ar is closer to the acceptor H_2S subunit in Structure B. At MP2/aug-cc-pVTZ level, the Ar-S distances R1 and R2 are 4.0543 and 3.6340 Å, respectively. In the pseudo-linear local minimum, C, the Ar atom interacts with the donor H_2S subunit, and the Ar-S distance R1 is 3.6643 Å at MP2/aug-cc-pVTZ level of theory. In both geometries, A

Table VI
Rotational constants (in MHz) for three minima optimized at different levels of theory

Structure		6-311++G**	6-311++G(3df,2p)	aug-cc-pVTZ	aug-cc-pVQZ	Experiment
A	*A*	–	1959.80	1994.59	1996.43	1810.410
	B	–	1646.92	1720.96	1722.66	1596.199
	C	–	900.85	930.21	931.09	848.814
B	*A*	1845.47	1971.72	2023.66	–	
	B	1566.47	1600.42	1663.89	–	
	C	854.03	890.72	919.83	–	
C	*A*	50227.41	68620.26	43894.38	44729.35	
	B	429.94	451.39	467.37	468.63	
	C	427.94	450.16	464.04	465.38	

and C, the $(H_2S)_2$ unit is not distorted much due to interaction with Ar. However, the distortion is more in B. Relative orientation of two H_2S subunits is changed in the presence of Ar in B. The free (non-H-bonded) H of the donor H_2S moiety is inclined towards Ar in B, as evident from Figs 3 and 4(b). The separation between two H_2S subunits (r) is similar for all three minima, the values being 4.0686, 4.0683 and 4.0775 Å for A, B and C, respectively, at MP2/aug-cc-pVTZ level of theory. Interestingly, the r value calculated for the H_2S–H_2S dimer is 4.0765 Å at the same level. Thus, structures A and B show a much smaller decrease of 0.01 Å in r, compared to the experimental estimate of 0.07 Å, discussed earlier. On the other hand, Structure C shows a very small increase of 0.001 Å compared to that in the dimer. Similar differences among the three structures are predicted with all basis sets used in this study.

The rotational constants for all the three geometries at different levels of theory, along with the experimentally obtained ones, are shown in Table VI. The experimental rotational constants can be correlated to those of structures A and B. However, the values of the calculated rotational constants should not be compared quantitatively with the experimental ones. The calculation gives the rotational constants for the equilibrium geometry at a particular level, whereas rotational constants of a vibrationally averaged structure are obtained in experiment.

It may be appropriate to discuss the rotational constants for the other state of Ar-$(H_2S)_2$ and Ar-$(D_2S)_2$ at this stage. The C rotational constants for lower and upper states are almost identical for both the isotopomers. The difference observed in $(A + B)/2$ between the two states for Ar-$(H_2S)_2$ is 12.29 MHz, whereas the same is only 45 kHz for Ar-$(D_2S)_2$. This is in contrast to the very similar difference observed in B rotational constants between the two states for $(H_2S)_2$ (1.20 MHz) and $(D_2S)_2$ (0.89 MHz) [18]. It appears that the two states of Ar-$(H_2S)_2$ that have been observed do not have a one-to-one correspondence with those of

Table VII
Interaction energies of the three minima optimized at different levels of theory for Ar-$(H_2S)_2$. ΔE^{CP} is the interaction energy after BSSE correction in counterpoise method. ΔE^{ZPE} is the interaction energy after correcting for zero point vibrational energy over ΔE^{CP}. All the energy values are in kcal mol^{-1}

Structure	Energy	6-311++G**	6-311++G(3df,2p)		aug-cc-pVTZ		aug-cc-pVQZ
		MP2	MP2	CCSD(T)	MP2	CCSD(T)	MP2
A	ΔE	–	–2.98	–2.58	–3.32	–2.88	–3.18
	BSSE	–	0.85	0.90	0.67	0.64	0.34
	ΔE^{CP}	–	–2.13	–1.68	–2.65	–2.24	–2.84
	ΔE^{ZPE}	–	–0.96	–0.51	–1.39	–0.98	–1.58
B	ΔE	–3.02	–2.94	–2.55	–3.21	–2.76	–
	BSSE	2.24	0.87	0.92	0.66	0.63	–
	ΔE^{CP}	–0.78	–2.07	–1.63	–2.55	–2.13	–
	ΔE^{ZPE}	0.69	–0.87	–0.43	–1.42	–1.00	–
C	ΔE	–2.60	–2.57	–2.25	–2.80	–2.44	–2.67
	BSSE	1.75	0.73	0.77	0.55	0.52	0.27
	ΔE^{CP}	–0.85	–1.83	–1.48	–2.25	–1.92	–2.40
	ΔE^{ZPE}	0.41	–0.75	–0.40	–1.12	–0.79	–1.27

$(H_2S)_2$. In the case of $(H_2O)_2$ and Ar-$(H_2O)_2$, a strong correlation could be established between the tunneling/internal rotor states observed in the two complexes [13]. A detailed discussion on the various states of $(H_2S)_2$ is beyond the scope of this work.

3.3.2. *Interaction energy*

The interaction energies (Ä*E*) are calculated using the super-molecule approach, and are corrected for basis set superposition error (BSSE) using the counterpoise (CP) method [22–24] to give the CP-corrected interaction energies (ΔE^{CP}) (Table VII). Single-point energy was calculated at CCSD(T) level for all three minima, optimized at MP2 level using 6-311++G(3f,2p) and aug-cc-pVTZ basis sets, using the same basis sets. Though the interaction energies for all three minima are comparable, the CP-corrected interaction energy for structure A is more than that for B and C at every level of calculation. However, the zero point energy corrected interaction energy at higher basis set (aug-cc-pVTZ) for minimum B is marginally (0.03 kcal/mol) higher than that for A. This is due to the lower zero point vibrational energy of B than that of A at this particular level of calculation. The CCSD(T) interaction energies are ~ 0.4 kcal/mol smaller than the corresponding MP2 values. The stabilization energies ($Ä E^{ZPE}$) for structures A, B and C are –0.98, –1.00 and –0.79 kcal/mol at CCSD(T)/aug-cc-pVTZ level of calculation. The BSSE decreases drastically on increasing the basis set. For structure C at MP2 level, BSSE goes down from a value of 1.75 kcal/mol for 6-311++G** basis set to 0.27 kcal/mol for aug-cc-pVQZ basis set.

3.3.3. *Vibrational frequencies*

Frequency calculations were performed for all optimized geometries to confirm the nature of the stationary points. All minima had only positive eigen values in the Hessian. The frequencies involving only the vibrations of H_2S units for all three geometries, calculated at MP2/aug-cc-pVTZ level, are listed in Table VIII. The corresponding vibrational frequencies of $(H_2S)_2$ dimer and the free monomer, calculated at the same level of theory, are also included in the table. In $(H_2S)_2$ dimer, the symmetric S–H stretch of the donor H_2S subunit undergoes a red-shift of ~ 42 cm^{-1}. In previous IR spectroscopic study of $(H_2S)_2$ in matrix, a shift of ~50 cm^{-1} was observed [25]. In Ar-$(H_2S)_2$, for B and C geometries there is a similar red shift in the same mode, whereas structure A undergoes a slightly higher shift, ~ 47 cm^{-1}.

Table VIII
Intramolecular H_2S vibrational frequencies for three minima (A, B, and C) for Ar-$(H_2S)_2$ along with the $(H_2S)_2$ dimer and free H_2S monomer frequencies calculated at MP2/aug-cc-pVTZ level. All values are in cm^{-1}

Modes	H_2S	$(H_2S)_2$	Ar-$(H_2S)_2$		
			A	B	C
Acceptor bend	1212	1209	1208	1208	1209
Donor bend		1216	1215	1215	1215
Donor symmetric stretch	2771	2729	2726	2730	2728
Acceptor symmetric stretch		2769	2768	2769	2769
Donor asymmetric stretch	2791	2783	2782	2784	2784
Acceptor asymmetric stretch		2789	2788	2790	2789

It appears from the theoretical results that the presence of Ar does not seriously alter the interactions in $(H_2S)_2$. It would be useful to get the experimental frequencies to confirm this. The donor asymmetric stretch also undergoes a small red shift for both $(H_2S)_2$ and Ar-$(H_2S)_2$. This may be contrasted with the Ar_2-H_2S trimer, which does not show any frequency shift [26]. In this trimer, though the Ar appears to interact through the H atoms in H_2S, there is no other signature of a 'hydrogen bond'.

4. Conclusions

The rotational spectra for Ar-$(H_2S)_2$ and Ar-$(D_2S)_2$ have been observed. Ar-$(H_2S)_2$ is an asymmetric top in the oblate limit, having the asymmetry parameter $k = 0.55$. Similar to $(H_2S)_2$, a two-state pattern has been observed for the trimer. The splitting in (A + B)/2 between the two states is 12.3 MHz for Ar-$(H_2S)_2$ and 45 kHz for Ar-$(D_2S)_2$. The spectra and the rotational constants are consistent with a T-shaped heavy atom vibrationally averaged geometry. The distance between the two H_2S units in Ar-$(H_2S)_2$ is determined to be 4.053 Å, which is 0.07 Å smaller than that in $(H_2S)_2$. The Ar-c.m(H_2S) distance is 4.085 Å, almost the same as that in Ar_2-H_2S complex. *Ab initio* calculations at MP2 and CCSD(T) level have also been performed using 6-311++G**, 6-311++G(3df,2p), aug-cc-pVTZ and aug-cc-pVQZ basis sets. These calculations lead to three minima. In these three minima, the Ar approaches towards $(H_2S)_2$ nominally along its *A*, *B* and *C* axes. Argon approaching along the *A* axis is a pseudo-linear geometry and has the least stabilization energy. The other two minima have a T-shaped heavy atom geometry. The experimental spectra are consistent with either of these two minima. At CCSD(T)/aug-cc-pVTZ level the minima having Ar along the *B/C* axss have a BSSE and zero-pint energy corrected stabilization energy of 1.0 kcal/mol. The theoretical vibrational frequency shift of donor H_2S indicates that both $(H_2S)_2$ and Ar-$(H_2S)_2$ are weakly H-bonded complexes.

Acknowledgement

The authors thank the Department of Science and Technology, New Delhi, India, for a generous grant and the Director of the Indian Institute of Science, Bangalore, India, for partial support. Partial support from the Council of Scientific and Industrial Research, India, is acknowledged. They also thank Mr A. P. Tiwari and Prof. P. C. Mathias and many others for their help in building the spectrometer, Dr Frank Lovas for providing with unpublished results on $(H_2S)_2$ and Ankit Jain for help with the user-interface program.

References

1. G. Scoles (ed.), *Atomic and molecular beam methods*, Vol. 1, Oxford University Press (1988).
2. G. Scoles (ed.), *Atomic and molecular beam methods*, Vol. 2, Oxford University Press (1992).
3. C. H. Townes, and A. L. Schawlow, *Microwave spectroscopy*, Dover (1975).
4. W. Gordy, and R. L. Cook, *Microwave molecular spectra*, Wiley (1984).
5. T. J. Balle, and W. H. Flygare, Fabry-Perot cavity pulsed Fourier transform microwave spectrometer with a pulsed nozzle particle source, *Rev. Sci. Instrumen.*, **52**, 33–45 (1981).
6. E. Arunan, S. Dev, and P. K. Mandal, Pulsed nozzle Fourier transform microwave spectrometer: Advances and applications, *Appl. Spectrosc. Rev.*, **39**, 131–181 (2004).

7. S. E. Novick, Bibliography of rotational spectra of weakly bound complexes, http://www.wesleyan.edu/chem/faculty/novick/vdw.html (2005).
8. S. E. Novick, P. Davies, S. J. Harris, and W. Klemperer, Determination of the structure of argon hydrogen chloride, *J. Chem. Phys.*, **59**, 2273–2279 (1973).
9. R. Viswanathan, and T. R. Dyke, The microwave and radiofrequency spectrum of hydrogen sulfide-agron complex (H_2S..Ar), *J. Chem. Phys.*, **82**, 1674–1681 (1985).
10. G. T. Fraser, F. J. Lovas, R. D. Suenram, and K. Matsumara, Microwave spectrum of argon-water: Dipole moment, isotopic studies, and oxygen-17 quadrupole coupling constants, *J. Mol. Spectrosc.*, **144**, 97–112 (1990).
11. E. Arunan, T. Emilsson, H. S. Gutowsky, and C. E. Dykstra, Rotational spectra and structures of the Ar_3-H_2O and Ar_3-H_2S symmetric tops, *J. Chem. Phys.*, **114**, 1242–1248 (2001).
12. E. Arunan, T. Emilsson, and H. S. Gutowsky, Rotational spectra, structure and dynamics of Ar_m-$(H_2O)_n$ clusters: Ar_2-H_2O, Ar_3-H_2O, Ar-$(H_2O)_2$ and Ar-$(H_2O)_3$. *J. Am. Chem. Soc.*, **116**, 8418–8419 (1994).
13. E. Arunan, T. Emilsson, and H. S. Gutowsky, Rotational spectra, structures and dynamics of small Ar_m-$(H_2O)_n$ clusters: The Ar-$(H_2O)_2$ trimer, *J. Chem. Phys.*, **116**, 4886–4895 (2002).
14. L. Pauling, *The nature of the chemical bond*, Cornell University Press (1960).
15. G. Desiraju, and T. Steiner, The weak hydrogen bond. In *Structural chemistry and biology*, Oxford University Press (1999).
16. M. Goswami, P. K. Mandal, D. J. Ramdass, and E. Arunan, Rotational spectra and structure of the floppy C_2H_4-H_2S complex: bridging hydrogen bonding and van der Waals interactions, *Chem. Phys. Lett.*, **393**, 22–27 (2004).
17. E. Arunan, A. P. Tiwari, P. K. Mandal, and P. C. Mathias, Pulsed nozzle Fourier transform microwave spectrometer: Ideal to define a hydrogen bond radius, *Curr. Sci.*, **82**, 533–540 (2002).
18. F. J. Lovas, R. D. Suenram, and L. H. Coudert, Rotational spectra of H_2S dimer, *43rd Int. Symp. on Molecular Spectroscopy*, Columbus, 1988. Also private communication with F. J. Lovas.
19. H. S. Gutwosky, T. E. Emilsson, and E. Arunan, Rotational spectra, structure and internal dynamics of Ar-H_2S isotopomers, *J. Chem. Phys.*, **106**, 5309–5315 (1997).
20. J. K. G. Watson, Determination of centrifugal distortion coefficients of asymmetric top molecules, *J. Chem. Phys.*, **46**, 1935–1949 (1967).
21. M. J. Frisch *et al*., *Gaussian 98*, Revision A.11.3, Gaussian, Inc., Pittsburgh, PA (2002).
22. S. F. Boys, and T. Bernardi, The calculation of small molecular interactions by the differences of separate total energies. Some procedures with reduced errors, *Mol. Phys.*, **19**, 553–566 (1970).
23. S. Simon, M. Duran, and J. J. Dannenberg, How does basis set superposition error change the potential surfaces for hydrogen-bonded dimers?, *J. Chem. Phys.*, **105**, 11024–11031 (1996).
24. I. Alkorta, I. Rozas, and J. Elguero, Non-conventional hydrogen bonds, *Chem. Soc. Rev.* **27**, 163–170 (1998).
25. G. de Oliviera, and C. E. Dykstra, Weakly bonded clusters of H_2S, *J. Mol. Structure* (*Theochem*), **362**, 275–282 (1996).
26. P. K. Mandal, *Rotational spectra of weakly bound H_2S complexes and hydrogen bond radius*. Ph. D. Thesis, Indian Institute of Science, Bangalore, India (2005).